Reversible control of Dzyaloshinskii-Moriya interaction at the graphene/Co interface via hydrogen absorption

Baishun Yang,[1] Qirui Cui,[1] Jinghua Liang,[1] Mairbek Chshiev,[2,*] and Hongxin Yang[1,3,†]

[1]*Ningbo Institute of Materials Technology and Engineering, Chinese Academy of Sciences, Ningbo 315201, China*

[2]*Univ. Grenoble Alpes, CEA, CNRS, Spintec, 38054 Grenoble, France*

[3]*Center of Materials Science and Optoelectronics Engineering, University of Chinese Academy of Sciences, Beijing 100049, China*

(Received 5 August 2019; published 7 January 2020)

Using first-principles calculations, we investigate the impact of hydrogenation on the Dzyaloshinskii-Moriya interaction (DMI) at graphene/Co interface. We find that both the magnitude and chirality of DMI can be controlled via hydrogenation absorbed on graphene surface. Our analysis using density of states combined with first-order perturbation theory reveals that the spin splitting and the occupation of Co-*d* orbitals, especially the d_{xz} and d_{z^2} states, play a crucial role in defining the magnitude and the chirality of DMI. Moreover, we find that the DMI oscillates with a period of two atomic layers as a function of Co thickness what could be explained by analysis of out-of-plane of Co orbitals. Our work elucidates the underlying mechanisms of interfacial DMI origin and provides an alternative route of its control for spintronic applications.

DOI: 10.1103/PhysRevB.101.014406

I. INTRODUCTION

Topological magnetic textures, such as magnetic skyrmions [1–6] and chiral domain walls [7,8] can be used as information carriers for next generation information storage and logic technologies thanks to their high stability, small size, and fast current driven mobility [9]. The Dzyaloshinskii-Moriya interaction (DMI) [10,11], which originates from spin-orbit coupling (SOC) in an inversion symmetry broken system, plays a crucial role in the formation of these topological magnetic textures. Specifically, it can influence the chirality as well as stability and migration velocity of chiral domain walls and skyrmions [6,7]. Therefore, finding an efficient approach to control the magnitude and chirality of DMI is beneficial for creation and manipulation these magnetic textures for graphene spintronic applications.

Recent reports indicate that the DMI can be induced at graphene/ferromagnetic metal interface [12,13]. Meanwhile, graphane, graphone, and one-third-hydrogenated graphene representing different proportion of C:H (1:1, 2:1 and 3:1, respectively) are successfully fabricated experimentally with large scale [14–17]. These experimental results imply the possibility of changing the concentration of H at graphene/ferromagnetic metal surface. Moreover, the smallest size, the lowest atomic weight and very weak binding energy of hydrogen make it attractive for devices employing hydrogen migration. Indeed, the modulation of hydrogen can significantly influence the magnetism of materials as reported, for instance, by Tan *et al.* who achieved 90° magnetization switching with H^+ insertion at the Co/GdO_x interface by external electric field [18]. Furthermore, it was also reported that multiferroics with strong magnetoelectric coupling was realized in antiferromagnetic $SrCoO_{2.5}$ through hydrogen intercalation [19]. Both experiments and theories made progress in tuning the DMI by changing materials, atomic layer stacking, insulator capping and external electric field, etc. [20–22]. However, a possibility of controlling the DMI via hydrogenation has not yet been reported.

In this paper, using first-principles calculations, we systematically investigated the behavior of DMI influenced by varying the concentration of H at graphene surface of graphene/Co structures. We found that the DMI oscillates with a period of about two monolayers (ML) as a function of Co film thickness. More importantly, we demonstrated that not only the strength but also the chirality of DMI could be controlled by changing the concentration of hydrogen absorption.

II. METHODS

The Dzyaloshinskii-Moriya interaction is calculated by employing the constrained spin-spiral supercell method [23]. Figure 1(a) shows the schematic diagram of hydrogenated graphene/Co structures with clockwise (CW) (left panel) and anticlockwise (ACW) (right panel) spin textures in one supercell. The ratio between H and C atom is varied from zero to half and to distinguish the concentration of the hydrogen atoms in the following, we label the five systems as Co@Gr, Co@Gr-1/8H, Co@Gr-2/8H, Co@Gr-3/8H, Co@Gr-4/8H, respectively. Please note that in following discussions on DMI sign and chirality we will always assume graphene on top of Co despite the aforementioned notations used for convenience and will adopt a positive (negative) DMI representing CW (ACW) chirality. All of our calculations are performed within the framework of density functional theory implemented in Vienna *ab initio* simulation package (VASP) [24–26]. The exchange-correlation potential is treated

*mair.chshiev@cea.fr

†hongxin.yang.spintec@gmail.com

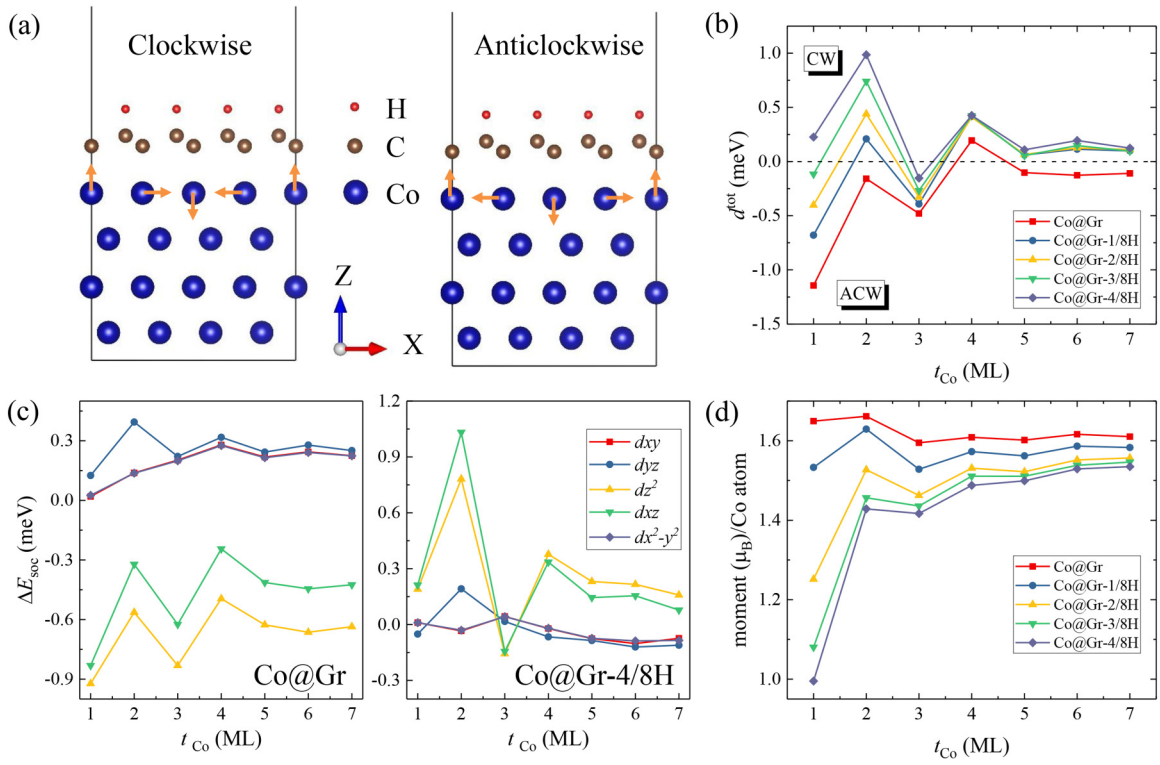

FIG. 1. (a) Schematic diagram of Co(4ML)@Gr-4/8H with CW and ACW spin textures. The arrows indicate spin orientations. (b) Calculated DMI as a function of Co thickness with different concentration of hydrogen on graphene surface. (c) SOC energy associated with DMI for Co@Gr and Co@Gr-4/8H as a function of Co thickness. (d) The average magnetic moment as a function of Co thickness with different concentration of hydrogen on graphene surface.

with the generalized gradient approximation with the Perdew-Burke-Ernzerhof functional [27]. The cutoff energy is set to 520 eV and a $6 \times 24 \times 1$ Γ-centered k-mesh is used in the calculations. A vacuum region larger than 15 Å is adopted in all the calculations to avoid the interaction between the neighboring slabs. The atomic positions are fully relaxed until the force and total energy is less than 0.001 eV/Å and 10^{-7} eV, respectively.

III. RESULTS AND DISCUSSION

The optimized Co(4ML)@Gr-4/8H slab is shown in Fig. 1(a). The distance between C and H is 1.13 Å, which is nearly the same as that in graphane and graphone [28]. With the absorption of hydrogen, the C atom bonding with H atom moves out of the plane toward H by 0.44 Å which makes the graphene not planar any more, while the cobalt atoms are still in the same plane. Figure 1(b) shows the calculated total DMI, d^{tot}, of graphene/Co with different concentration of H absorption when the thickness of Co varies from 1 to 7 ML. One can see that in all cases the DMI oscillates with a period of 2 ML as a function of Co film thickness up to 5 ML beyond which the DMI strength nearly stabilizes at constant values. Furthermore, the magnitude of DMI gradually increases as a function of hydrogen concentration and even changes its sign in some cases. For example, the DMI strength in Co(1ML)@Gr is −1.14 meV and it reverses its sign and decreases to 0.23 meV in Co(1ML)@Gr-4/8H.

Considering that the oscillatory DMI behavior is a common feature in all systems considered here, we suppose that this phenomenon is not due to hydrogen. The oscillatory behavior as a function of film thickness due to quantum well states (QWS) occurs for different physical phenomena such as magnetocrystalline anisotropy [29–31], Curie temperature [32] and magnetic exchange coupling [33–35]. In particular, similar oscillation period of 2 ML for magnetic anisotropy energy of Co slabs and magnetic coupling of MnGa/Co(Fe) and Cu/Co(Fe) films are reported in Refs. [36–38]. Details of this QWS in Co film are considered to be arising from the electronic states reflected from top and bottom Co surfaces. The DMI of graphene/Co interface is induced by the Rashba effect with the SOC energy localized on Co atoms [12]. In order to elucidate the orbital contribution to DMI oscillations, in Fig. 1(c) we show the associated SOC energy dependences as a function of Co thickness resolved for each d orbital of Co atoms. It can be seen that for both Co@Gr and Co@Gr-4/8H systems, the associated SOC energy arising from d_{xz} and d_{z^2} has an oscillation period of 2 ML with a large amplitude, so does the d_{yz} orbital but with a smaller amplitude. In contrast, the SOC energy contributions from in-plane d_{xy} and $d_{x^2-y^2}$ orbitals are almost degenerated in respect to each other and have almost no change as a function of Co thickness. Thus, the oscillations of DMI is determined by the $d_{z^2(xz,\,yz)}$ states of Co film that could be attributed to much stronger impact of interfaces on out-of-plane orbitals compared to the in-plane ones.

Let us now investigate other physical mechanisms explaining the DMI variation as function of hydrogenation. Belabbes *et al.* [22] demonstrated that besides the SOC, the electronic occupation of magnetic atom also strongly affects the DMI. In particular, the DMI in $3d/5d$ interfaces follows Hund's rule with a similar tendency to their magnetic moments [22]. To verify whether the underlying mechanism of the DMI change in our case is associated with the magnetic moment variation, we plot the corresponding average magnetic moment of each of the systems in Fig. 1(d). One can see that the average magnetic moment of Co decreases monotonically as hydrogen concentration increases with significantly more pronounced impact for thin Co films. For instance, the magnetic moment of Co drops from $1.65\,\mu_B$ in Co(1ML)@Gr to $1.00\,\mu_B$ in Co(1ML)@Gr-4/8H due to the strong interfacial hybridization between H and C. For large Co thicknesses, the magnetic moments stabilize within a narrow interval between 1.55 and $1.60\,\mu_B$. Interestingly, in most of the cases of thin Co films the average magnetic moment also shows oscillatory behavior with a period of 2ML. Most importantly, there is a clear correlation between the magnetic moment and DMI curves. Namely, a higher concentration of hydrogen clearly diminishes both the DMI and the magnetic moments. This suggests that the DMI also follows the Hund's rule here. However, the sign of DMI does not follow the trend of magnetic moment variation. Therefore, the Hund's rule cannot fully explain the DMI behavior here and one should seek for further physical mechanisms.

In order to elucidate the origin of the sign and strength change of DMI by hydrogen absorption, we can now employ the analysis based on noncollinear Hamiltonian treated in the framework of the first-order perturbation theory [39–41]. The corrections to the total energy due to DMI can be approximated by the expectation value of the corresponding term written as $\langle\psi_{lm,s}|\xi\boldsymbol{\sigma L}|\psi_{lm,s}\rangle$ where $|\psi_{lm,s}\rangle = \sum|Y_{lm},\,\chi_s\rangle$ represents the quantum state comprising eigenstates Y_{lm} and χ_s of orbital momentum and spin operators, respectively. Here l, m, and s represent orbital, magnetic and spin quantum numbers, respectively. In our case, as shown in Figs. 1(a) and 1(b), the spins lie in x-z plane, $\xi\sigma_x L_x$ and $\xi\sigma_z L_z$ components will cancel with each other, therefore, only the y component $\langle\psi_{lm,s}|\xi\sigma_y L_y|\psi_{lm,s}\rangle$ needs to be considered [42]. Based on first-order perturbation theory, all of the occupied states contribute to the corrected total energy. For instance, following the analysis of SOC matrix elements between fully occupied different d orbitals and spins, we find that the expectation value of $\langle d_{z^2}\chi_+ + d_{xz}\chi_-|\sigma_y L_y|d_{z^2}\chi_+ + d_{xz}\chi_-\rangle$ and $\langle d_{z^2}\chi_- + d_{xz}\chi_+|\sigma_y L_y|d_{z^2}\chi_- + d_{xz}\chi_+\rangle$ are, respectively, equal to $-\sqrt{6}$ and $\sqrt{6}$ giving the highest contribution to the DMI. In contrast, other nonzero matrix elements $\langle d_{xy}\chi_+ + d_{yz}\chi_-|\sigma_y L_y|d_{xy}\chi_+ + d_{yz}\chi_-\rangle$, $\langle d_{xz}\chi_+ + d_{x^2-y^2}\chi_-|\sigma_y L_y|d_{xz}\chi_+ + d_{x^2-y^2}\chi_-\rangle$, $\langle d_{xy}\chi_- + d_{yz}\chi_+|\sigma_y L_y|d_{xy}\chi_- + d_{yz}\chi_+\rangle$ and $\langle d_{xz}\chi_- + d_{x^2-y^2}\chi_+|\sigma_y L_y|d_{xz}\chi_- + d_{x^2-y^2}\chi_+\rangle$ are equal to $\sqrt{2}$, $-\sqrt{2}$, $-\sqrt{2}$ and $\sqrt{2}$, respectively. Using the properties of rotation and Pauli spin matrices one can deduce that positive (negative) sign of matrix element of $\sigma_y L_y$ operator corresponds to the CW (ACW) chirality of the DMI. Interestingly, a similar analysis can be performed for magnetic anisotropy in the framework of second-order perturbation theory [43,44].

From the first-order perturbation theory, we can conclude that the occupation states change of Co will have a large influence on the DMI. In Figs. 2(a)–2(d) we show the projected density of states (DOS) of Co atom in Co(1ML)@Gr, Co(1ML)@Gr-1/8H, Co(1ML)@Gr-2/8H, and Co(1ML)@Gr-4/8H. Due to the coverage of hydrogenated graphene on Co film, the Jahn-Teller distortion lowers the symmetry from D_{3d} of pure Co film to C_{3v} of Co(1ML)@Gr and Co(1ML)@Gr-4/8H and finally decreases to C_s symmetry (i.e., no symmetry) of Co(1ML)@Gr-1/8 and Co(1ML)@Gr-2/8. Therefore, the fivefold degenerated $3d$ electron states split into three irreducible representations, doublet degenerate level e_1 (d_{yz}, d_{xz}), e_2 (d_{xy}, $d_{x^2-y^2}$) and a singlet a state (d_{z^2}) in C_{3v} and D_{3d} point group. For C_s symmetry, the e_1 and e_2 states are further broken as their corresponding orbitals split into nondegenerate states. For convenience, since the splitting of these states in C_s symmetry has no dramatic influence on the DMI in our calculations, only d_{xy}, d_{xz} and d_{z^2} states for Co(1ML)@Gr-1/8H and Co(1ML)@Gr-2/8H systems are plotted in Figs. 2(b) and 2(c). Summarizing the variation of DOS with increase of H concentration in Fig. 2, one can note two characteristic features. First, bonding between Co and graphene gets stronger when H absorbed on graphene as d states become more localized. Second, spin splitting decreases leading to smaller magnetic moments as seen in Fig. 1(d). As a result, the antibonding majority d_{z^2} (minority d_{xz}) electronic states shift upward (downward) in energy with a decrease (increase) of their occupation. To better understand and visualize these findings on the influence of exchange splitting and crystal field on electronic states of Co, we plot the corresponding schematic diagram of the Co d states energy levels in Co(1ML)@Gr and Co(1ML)@Gr-4/8H [Figs. 2(e) and 2(f)]. Note that e_2 (d_{xy}, $d_{x^2-y^2}$) states are spread across large region in energy (these energy levels are not shown). By comparing the two cases, one can see indeed that the majority d_{z^2} states become less occupied since its antibonding state moves above the Fermi level (top brown line). Also, it clearly follows that the exchange splitting is smaller in case of Co(1ML)@Gr-4/8H. This also explains why a higher concentration of hydrogen absorption on graphene surface generates a lower magnetic moment in graphene/Co systems.

The trend in DMI behavior as a function of hydrogen concentration can then be understood from the analysis of projected DOS for Co(1ML)@Gr shown in Fig. 2. One can see that only d_{xz} minority and d_{z^2} majority states are mostly affected by hydrogenation. Namely, increasing H concentration leads to increasing (decreasing) of d_{xz} minority (d_{z^2} majority) states occupation [Figs. 2(a)–2(d)] so that among aforementioned matrix elements of SOC operator one should focus on the first one, i.e., $\langle d_{z^2}\chi_+ + d_{xz}\chi_-|\sigma_y L_y|d_{z^2}\chi_+ + d_{xz}\chi_-\rangle$, which corresponds to ACW chirality. Since the decreasing rate of d_{z^2} majority occupation is higher than the increasing rate of d_{xz} minority occupation, this SOC matrix element has an overall tendency to decrease. This causes lower DMI of ACW chirality for system without and with 1/8, 2/8, and 3/8 hydrogenation and eventual DMI change to CW chirality for Co(1ML)@Gr-4/8H [cf. Figs. 1(b) and 2(a)–2(d)]. To further confirm this behavior, in Fig. 3 we plot the orbital resolved contributions to DMI deduced from SOC matrix elements for Co(1ML)@Gr and Co(1ML)@Gr-4/8H. It is clear that the

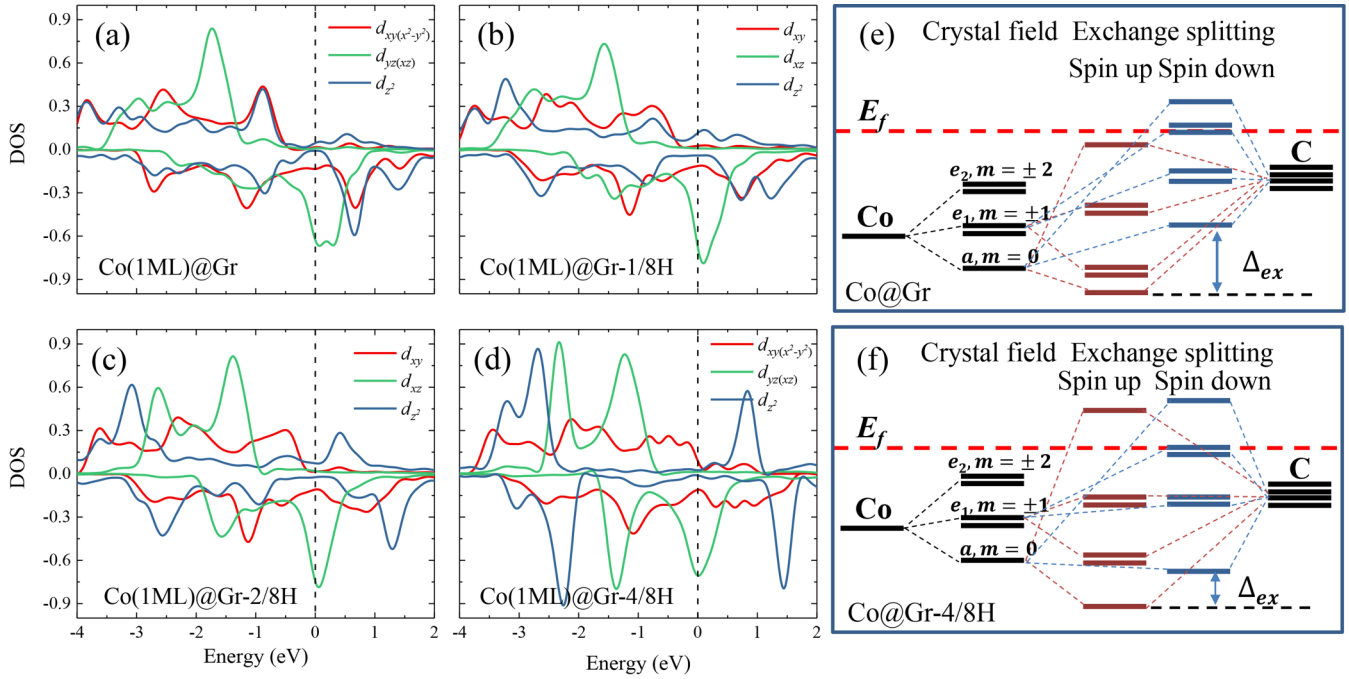

FIG. 2. (a)–(d) The density of states of Co in graphene/Co(1ML) systems with different concentration of hydrogen. The schematic diagram of energy levels of Co in (e) Co@Gr and (f) Co@Gr-4/8H.

strongest contribution to DMI comes indeed from the matrix element with d_{xz} and d_{z^2} orbitals, which is strongly negative and positive for Co(1ML)@Gr and Co(1ML)@Gr-4/8H as shown in Figs. 3(a) and 3(b), respectively.

To further verify the reliability of proposed fundamental mechanism responsible for strength and sign of DMI in hydrogenated Co@Gr structure, in Fig. 4 we present projected DOS of interfacial Co atom in structures with thicker Co, i.e., Co(7ML)@Gr and Co(7ML)@Gr-4/8H. Similar to structures with 1ML Co, two characteristic features, i.e., enlarged bonding between Co and carbon as well as the decreased spin splitting, are also observed in the 7ML Co structures. The DMI behavior is also similar giving ACW and CW DMI for Co(7ML)@Gr and Co(7ML)@Gr-4/8H, respectively. Thus, we conclude that occupation of electronic states, notably d_{xz} and d_{z^2}, are crucial for the strength and the sign of DMI, and their modulation is essential in controlling DMI.

IV. CONCLUSION

In summary, using first principles calculations we have systematically investigated the effect of hydrogenation on

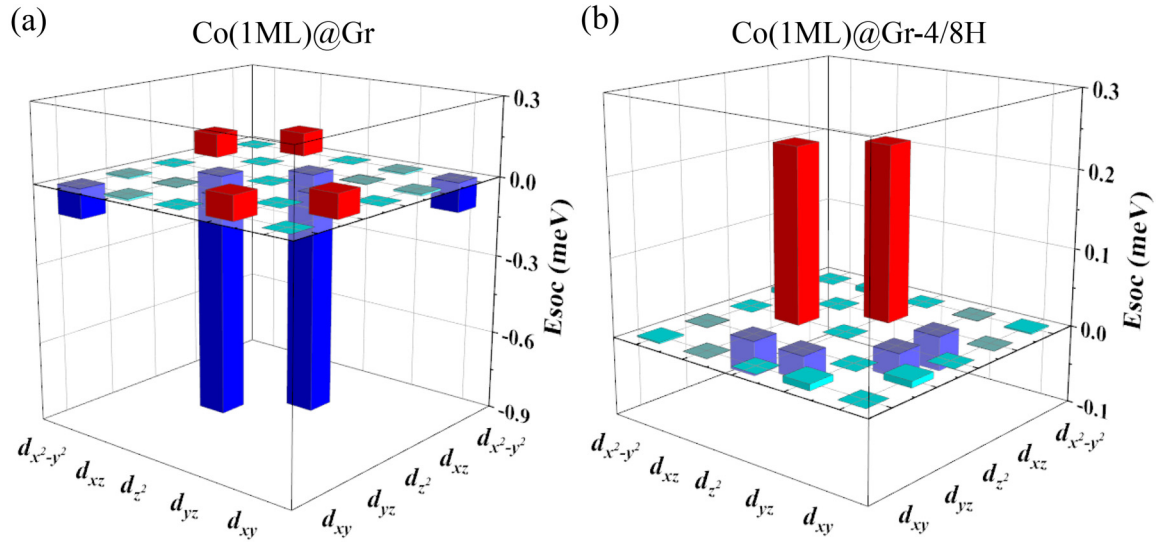

FIG. 3. Orbital resolved SOC energy matrix elements associated with DMI of Co in (a) Co(1ML)@Gr and (b) Co(1ML)@Gr-4/8H, respectively.

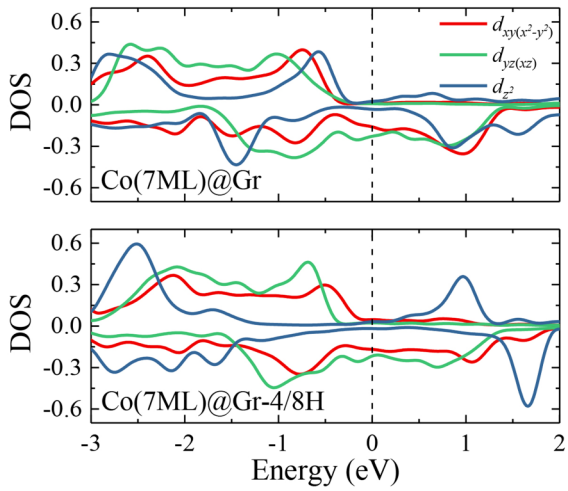

FIG. 4. The DOS of surface Co atom in (a) Co(7ML)@Gr and (b) Co(7ML)@Gr4/8H, respectively.

DMI by using Co@Gr as a prototype system. We found that the DMI oscillates with a period of two ML as a function of Co film thickness. The DMI oscillations are mainly due to out-of-plane $d_{z^2(xz,\ yz)}$ orbitals. Furthermore, as hydrogen concentration increases, the ACW DMI decreases and eventually changes its chirality to CW. This behavior can be explained in the framework of the first-order perturbation theory via analysis of occupation states of d_{xz} and d_{z^2} orbitals. This provides a promising method for controlling the spin-orbitronic phenomena such as the formation of domain walls and skyrmions. Moreover, our understanding of the DMI will serve as a guideline for experimental and theoretical investigations on the chiral magnetic systems.

ACKNOWLEDGMENTS

This work was supported by the National Natural Science Foundation of China (11874059), Zhejiang Province Natural Science Foundation of China (LR19A040002), the Ningbo 3315 project, Horizon 2020 Research and Innovation Programme under Grant No. 785219 (Graphene Flagship), and the China Postdoctoral Science Foundation (2019M652151). The work was carried out at National Supercomputer Center in Tianjin, and the calculations were performed on TianHe-1 (A).

[1] U. K. Rößler, A. N. Bogdanov, and C. Pfleiderer, Nature (London) **442**, 797 (2006).
[2] S. Mühlbauer, B. Binz, F. Jonietz, C. Pfleiderer, A. Rosch, A. Neubauer, R. Georgii, and P. Böni, Science **323**, 915 (2009).
[3] X. Z. Yu, Y. Onose, N. Kanazawa, J. H. Park, J. H. Han, Y. Matsui, N. Nagaosa, and Y. Tokura, Nature (London) **465**, 901 (2010).
[4] A. Fert, V. Cros, and J. Sampaio, Nat. Nanotechnol. **8**, 152 (2013).
[5] C. Pappas, E. Lelievre-Berna, P. Falus, P. M. Bentley, E. Moskvin, S. Grigoriev, P. Fouquet, and B. Farago, Phys. Rev. Lett. **102**, 197202 (2009).
[6] A. Fert, N. Reyren, and V. Cros, Nat. Rev. Mater. **2**, 17031 (2017).
[7] A. Thiaville, S. Rohart, É. Jué, V. Cros, and A. Fert, Europhys. Lett. **100**, 57002 (2012).
[8] K.-Su Ryu, L. Thomas, S.-H. Yang, and S. Parkin, Nat. Nanotechnol. **8**, 527 (2013).
[9] A. Soumyanarayanan, N. Reyren, A. Fert, and C. Panagopoulos, Nature (London) **539**, 509 (2016).
[10] I. Dzyaloshinsky, J. Phys. Chem. Solids **4**, 241 (1958).
[11] T. Moriya, Phys. Rev. **120**, 91 (1960).
[12] H. Yang, G. Chen, A. A. C. Cotta, A. T. N'Diaye, S. A. Nikolaev, E. A. Soares, W. A. A. Macedo, K. Liu, A. K. Schmid, A. Fert, and M. Chshiev, Nat. Mater. **17**, 605 (2018).
[13] F. Ajejas, A. Gudín, R. Guerrero, A. A. Barcelona, J. M. Diez, L. M. Costa, P. Olleros, M. A. Niño, S. Pizzini, J. Vogel, M. Valvidares, P. Gargiani, M. Cabero, M. Varela, J. Camarero, R. Miranda, and P. Perna, Nano. Lett. **18**, 5364 (2018).
[14] D. C. Elias, R. R. Nair, T. M. G. Mohiuddin, S. V. Morozov, P. Blake, M. P. Halsall, A. C. Ferrari, D. W. Boukhvalov, M. I. Katsnelson, A. K. Geim, and K. S. Novoselov, Science **323**, 610 (2009).
[15] Y. Wang, X. Xu, J. Lu, M. Lin, Q. Bao, B. Özyilmaz, and K. P. Loh, ACS Nano **4**, 6146 (2010).
[16] R. Balog, B. Jørgensen, L. Nilsson, M. Andersen, E. Rienks, M. Bianchi, M. Fanetti, E. Lægsgaard, A. Baraldi, S. Lizzit, Z. Sljivancanin, F. Besenbacher, B. Hammer, T. G. Pedersen, P. Hofmann, and Liv Hornekær, Nat. Mater. **9**, 315 (2010).
[17] H. Chen, D. Bao, D. Wang, Y. Que, W. Xiao, G. Qian, H. Guo, J. Sun, Y. Zhang, S. Du, S. T. Pantelides, and H.-J. Gao, Adv. Mater. **30**, 1801838 (2018).
[18] A. J. Tan, M. Huang, C. O. Avci, F. Büttner, M. Mann, W. Hu, C. Mazzoli, S. Wilkins, H. L. Tuller, and G. S. D. Beach, Nat. Mater. **18**, 35 (2019).
[19] J. Y. Ni, P. S. Wang, J. L. Lu, and H. J. Xiang, Phys. Rev. Lett. **122**, 117601 (2019).
[20] A. Belabbes, G. Bihlmayer, S. Blügel, and A. Manchon, Sci. Rep. **6**, 24634 (2016).
[21] H. Yang, O. Boulle, V. Cros, A. Fert, and M. Chshiev, Sci. Rep. **8**, 12356 (2018).
[22] A. Belabbes, G. Bihlmayer, F. Bechstedt, S. Blügel, and A. Manchon, Phys. Rev. Lett. **117**, 247202 (2016).
[23] H. Yang, A. Thiaville, S. Rohart, A. Fert, and M. Chshiev, Phys. Rev. Lett. **115**, 267210 (2015).
[24] G. Kresse and J. Furthmüller, Phys. Rev. B **54**, 11169 (1996).
[25] G. Kresse and J. Furthmüller, Comput. Mater. Sci. **6**, 15 (1996).
[26] G. Kresse and J. Hafner, Phys. Rev. B **47**, 558 (1993).
[27] J. P. Perdew, K. Burke, and M. Ernzerhof, Phys. Rev. Lett. **77**, 3865 (1996).
[28] B. S. Pujari, S. Gusarov, M. Brett, and A. Kovalenko, Phys. Rev. B **84**, 041402(R) (2011).
[29] J. Li, M. Przybylski, F. Yildiz, X. D. Ma, and Y. Z. Wu, Phys. Rev. Lett. **102**, 207206 (2009).
[30] T. R. Dasa, P. Ruiz-Díaz, O. O. Brovko, and V. S. Stepanyuk, Phys. Rev. B **88**, 104409 (2013).

[31] M. Dąbrowski, T. R. F. Peixoto, M. Pazgan, A. Winkelmann, M. Cinal, T. Nakagawa, Y. Takagi, T. Yokoyama, F. Bisio, U. Bauer, F. Yildiz, M. Przybylski, and J. Kirschner, Phys. Rev. Lett. **113**, 067203 (2014).
[32] M. Pajda, J. Kudrnovský, I. Turek, V. Drchal, and P. Bruno, Phys. Rev. Lett. **85**, 5424 (2000).
[33] S. S. P. Parkin, R. Bhadra, and K. P. Roche, Phys. Rev. Lett. **66**, 2152 (1991).
[34] J. E. Ortega and F. J. Himpsel, Phys. Rev. Lett. **69**, 844 (1992).
[35] Z. Q. Qiu, J. Pearson, A. Berger, and S. D. Bader, Phys. Rev. Lett. **68**, 1398 (1992).
[36] R. Coehoorn, Phys. Rev. B **44**, 9331 (1991).
[37] J. Tong, L. Ruan, X. Yao, F. Tian, G. Qin, and X. Zhang, Phys. Rev. B **97**, 184426 (2018).
[38] M. Cinal, J. Phys.: Condens. Matter **15**, 29 (2003).
[39] P. Kurz, F. Förster, L. Nordström, G. Bihlmayer, and S. Blügel, Phys. Rev. B **69**, 024415 (2004).
[40] M. Heide, G. Bihlmayer, and S. Blugel, Phys. Rev. B **78**, 140403(R) (2008).
[41] V. Kashid, T. Schena, B. Zimmermann, Y. Mokrousov, S. Blügel, V. Shah, and H. G. Salunke, Phys. Rev. B **90**, 054412 (2014).
[42] M. Heide, G. Bihlmayer, and S. Blügel, Physica B **404**, 2678 (2009).
[43] D.-S. Wang, R. Wu, and A. J. Freeman, Phys. Rev. B **47**, 14932 (1993).
[44] B. S. Yang, J. Zhang, L. N. Jiang, W. Z. Chen, P. Tang, X. G. Zhang, Y. Yan, and X. F. Han, Phys. Rev. B **95**, 174424 (2017).